An Efficient Indoor Target Tracking Algorithm Using TDOA Measurements With Applications to Ultra-Wideband Systems

HYUNG JUNE KIM[1], YIFAN XIE[1], HEEKWON YANG[2], CHANKIL LEE [2], (Senior Member, IEEE), AND TAEK LYUL SONG [1], (Senior Member, IEEE)

[1]Department of Electronic Systems Engineering, Hanyang University, Ansan 15588, South Korea
[2]Department of Electronics and Communication, Hanyang University, Ansan 15588, South Korea

Corresponding author: Taek Lyul Song (tsong@hanyang.ac.kr)

ABSTRACT The ultra-wideband technique has shown its effectiveness for indoor target tracking. Various types of measurements have been applied to ultra-wideband systems for indoor target tracking, and the time difference of arrival (TDOA) measurement-based approaches are the most widely used methods due to their good accuracy and feasibility. Target tracking with the TDOA measurements usually encounters the problem of correlated measurement noises, as one sensor network utilizes the common reference sensor for measurement generation. The off-diagonal entries in the measurement error covariance matrix become non-zero values, which makes the standard target tracking algorithms inconvenient for practical installation of an ultra-wideband system. Another problem in sensor networks is properly exploiting the measurements obtained from multiple sensors considering practical conditions, such as storage limitations or computational resource consumption. The parallel update and the serial update are usually applied for the multi-sensor tracking problem. This paper presents a target tracking algorithm that integrates the Cholesky decomposition to decorrelate the measurement noises for the serial update, thus improving computational efficiency. The proposed algorithm is realized in an ultra-wideband system for real-time target tracking, and an experiment using real data is conducted to validate its practicability.

INDEX TERMS Target tracking, TDOA, UWB, correlated noise.

I. INTRODUCTION

Indoor target tracking has emerged as a critical role in civilian and military applications such as aiding tourists in entertainment venues, locating confidential devices and providing navigation services, [1]–[4]. Numerous techniques such as radio frequency identification (RFID), infrared (IR), blue tooth, and ultra wideband (UWB) have been studied for indoor target tracking over the past decades. RFID-based approaches usually suffer from a lack of communication capabilities and small positioning coverage. The main drawback of IR-based approaches is that the IR communications are usually blocked by obstacles, as IR signals cannot penetrate through walls. The spectrum that blue-tooth uses is unlicensed such that radio interference from other devices occurs frequently. In contrast, the applications of UWB technique are strictly regulated. Thus the use of wide range UWB frequency is usually limited to reduce the possibility of radio interference and frameworks for UWB communication are developed individually. Additionally, the high bandwidth and extremely short pulses of the UWB system contribute to determinations of signal arrival time and reduction of multi-path interference effects, making UWB a more desirable technique for indoor target tracking systems.

UWB tracking systems can utilize various information obtained from the received signals, which include received signal strength (RSS), angle of arrival (AOA), time of arrival (TOA), and time difference of arrival (TDOA). Hybrid schemes that use combinations of the above signals can provide more accurate information about the target position. For practical installations, the measurement type selection depends on computational constraints and

The associate editor coordinating the review of this manuscript and approving it for publication was Lubin Chang.

accuracy requirements [5]. The UWB signal usually suffers from path loss (the ratio of the received signal power to the transmitted power) when traveling from one sensor to another. Because the RSS measurement accuracy relies on the received power and the path loss attenuates the radio signals, the RSS measurement defines an area of uncertainty instead of a circle [6]. The AOA measurement accuracy is sensitive to the distance between the target and the sensor. A small error in angle can lead to a large uncertainty area (circular sector) when the target is remote from the sensor. The UWB signal provides a very large bandwidth. This property contributes to a highly precise time resolution such that TOA and TDOA measurements benefit from higher accuracy relative to other measurement types. The performance of a TOA-based system is considerably affected by clock synchronization since all sensors should be synchronized precisely, which limits its applicability [7]. In contrast, the superiority of TDOA measurement includes its smaller requirements for clock synchronization, where only the reference sensor and the measured sensor have to be synchronized [4].

In a wireless sensor network (WSN), each sensor forwards the received target signal such as TOA to a centralized fusion center where the target location is estimated. The TDOA information can be extracted from the collected TOAs via two methods: (1) calculating the difference between the two TOAs; (2) performing a generalized cross-correlation (GCC) technique among TOAs [5]. Although the TOA measurement noises in one WSN are mutually uncorrelated, as each sensor operates independently, the first TDOA generation method designates one sensor as the common reference sensor and the TDOA measurement noises become correlated. Most of the multi-sensor target tracking algorithms [8]–[10] are developed based on the uncorrelated measurement noise assumption, which is not the case in reality. Reference [11] points out that neglecting the noise correlation can lead to a mismatch between the real measurement uncertainty coverage and the estimated one, which further results in an inaccurate tracking performance.

The noise correlation also causes another multi-sensor fusion problem. Measurements from different sensors are usually handled by two approaches: the parallel update and the serial update [12]. References [8], [13] and [14] show that the two approaches are mathematically equivalent and deliver identical results under two conditions: (1) the system is linear; (2) the measurement noise is uncorrelated. Since the TDOA measurement equation is nonlinear and the TDOA measurement noise is correlated, these two conditions cannot be satisfied in practice. The measurement nonlinearity can be linearly approximated by an extended Kalman filter (EKF), but the linearization step introduces different approximation errors between parallel update and serial update [15]. The noise correlation turns the off-diagonal entries in the measurement error covariance matrix into non-zero values, and the serial update cannot be applied directly. The parallel update utilizes all measurements simultaneously by augmenting the measurement state vector as well as the

corresponding error covariance matrices, making it immune to noise correlation. Because of the correlated nature of the measurement error covariance, the serial update suffers from losses in information and tracking accuracy without an appropriate noise decorrelation approach [16]. Numerous studies have been focused on the correlated TDOA measurement noise [17]–[19]. Reference [18] investigates the relationship between the variance of measurement noise and the parameters such as signal-to-noise ratio (SNR), bandwidth and frequency of the received signals. Reference [19] applies the Gram-Charlier orthogonalization to decorrelate the measurement noise in the first step, then approximates the measurement likelihood function by a Gaussian mixture instead of one Gaussian distribution. The Gaussian mixture approximation in [19] improves the precision in modeling the measurement uncertainty area at the cost of more storage requirements and computational complexity.

In this paper, the application of Cholesky decomposition [16], [20], [21] removes the noise correlation such that the serial update can be directly implemented with the decorrelated TDOA measurement. TDOA measurement noise decorrelation is achieved by modifying the standard measurement vector, predicted measurement vector and the standard Jacobian matrix with the inverse of the decomposition matrix. Precomputation for all entries in the inverse of unit lower triangular matrix avoids complicated matrix computations so that computational efficiency can be substantially improved. Experiments using real data from a UWB system are also conducted to verify the practicability of the proposed algorithm.

The rest of the paper is organized as follows. The state vector definition and the TDOA measurement noise correlation are presented in Section II. Section III describes the details of the Cholesky decomposition and its application to noise decorrelation. The EKF parallel update and the proposed EKF serial update using the decorrelated TDOA measurements are discussed in Section IV. Simulation studies for indoor target tracking of the proposed method are given in Section V, followed by descriptions for the corresponding experiment in Section VI.

II. PROBLEM STATEMENTS

In the problem of passive source localization using TDOA measurements, the signal is transmitted from the device mounted on a target and is received by each sensor at different instances. The difference in arrival time between two sensors can be converted into the difference in distances between the target and the two sensors by multiplying with the signal propagation speed, which generates one range difference of arrival (RDOA) measurement. One RDOA measurement defines a hyperbola in 2D or a hyperboloid in 3D. Every position on the hyperbola or hyperboloid indicates a possible target location such the target observability cannot be satisfied when only one TDOA measurement is provided. In 2D environments, a minimum of 2 TDOA measurements are required to locate a target, where the intersection of two hyperbolas defines the target location as illustrated in Fig. 1;
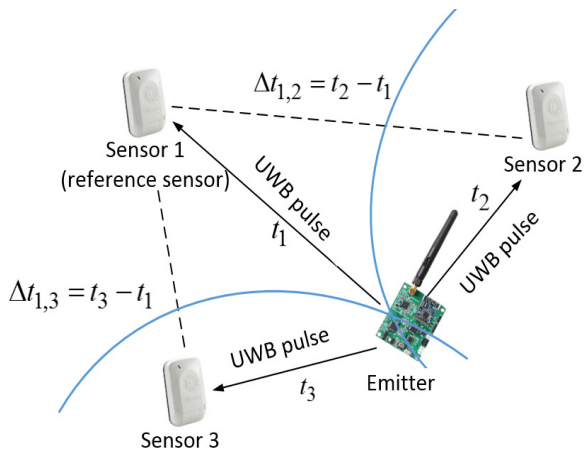
FIGURE 1. Example of a UWB real-time localization system in 2D.

whereas in 3D environments, the target is localized by the intersections of three hyperboloids, i.e., 3 TDOA measurements are required.

A. UWB SIGNAL INFORMATION

In a UWB-based tracking system, ranging packets from targets must be identified and guaranteed against collisions. According to IEEE standard 802.15.4 beacon-enabled medium access control (MAC) and high rate pulse repetition frequency (HRP) UWB ranging packet format, a simplified time-division multiple access (TDMA) MAC is used in this study and a target identification number is included in the payload of a ranging packet as shown in Fig. 2.
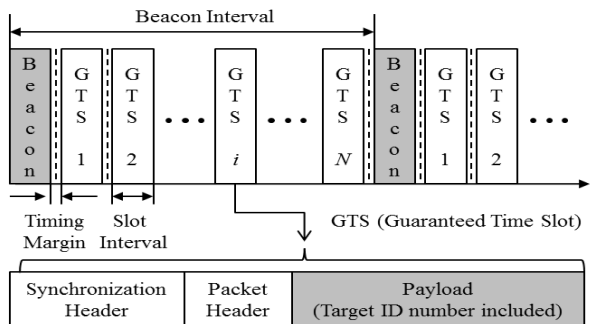

FIGURE 2. Channel access method and ranging packet format.

The reference sensor broadcasts beacon signal periodically to synchronize the sensor clocks. To prevent a guaranteed time slot (GTS) from overlapping adjacent one, the timing margin is introduced between GTSs. Time-stamps indicating the arrival time at the sensor are collected wirelessly by a reference sensor and transmitted to a localization server.

The existence of target ID number in each GTS identifies the signal origin so that the measurement origin uncertainty problem is solved. Additionally, the measurement-to-track data association algorithm which is usually required in

multiple-target scenarios becomes unnecessary as the measurement origins are known.

B. STATE VECTOR

Under the additive noise assumption, the motion of the target at scan k is modeled as a linear-Gaussian in Cartesian coordinates as

$$e_k = F_k e_{k-1} + \omega_k, \tag{1}$$

where $e_k = [x_k \; \dot{x}_k]^T$ is the target state vector composed by a position component x_k and a velocity component $\dot{x}_k$, F_k denotes the transition matrix, and ω_k is the white Gaussian process noise with zero mean and covariance matrix Q_k.

The sensor network is constituted by stationary sensors at predetermined positions with state vectors $e_k^i = [x_k^i \; 0_3]^T$ ($i = 1, \ldots, M$), where M is the total number of sensors and 0_n denotes the $n \times n$ zero matrix. The distance vector between the target and the i-th sensor is $r_{k,i} = x_k - x_k^i$, and $||r_{k,i}||$ is the corresponding Euclidean distance.

C. TDOA MEASUREMENT

Assume that sensor s_1 is utilized as the common reference sensor in this sensor network for TDOA measurement generation. Multiplying with the signal propagation speed c, the TDOA measurement is converted into a range difference such that

$$z_{k,i} = (||r_{k,i}|| - ||r_{k,1}||) + c(u_{k,i} - u_{k,1}) \tag{2}$$
$$= h_i(e_k) + v_{k,i}, \quad i = 2, 3, \ldots, M \tag{3}$$

where $u_{k,i} \sim \mathcal{N}(0, (\sigma_i/c)^2)$ is denoted as the Gaussian noise of sensor s_i and

$$h_i(e_k) = ||r_{k,i}|| - ||r_{k,1}||, \tag{4}$$
$$v_{k,i} = c(u_{k,i} - u_{k,1}), \tag{5}$$

where $v_{k,i} \sim \mathcal{N}(0, \sigma_{1,i}^2)$ is the TDOA measurement noise with standard covariance $\sigma_{1,i}^2 = \sigma_1^2 + \sigma_i^2$.

As s_1 is utilized as the reference sensor, $M-1$ TDOA measurements are created at each scan k, which can be presented by a stacked form of

$$z_k = [z_{k,2} \; z_{k,3} \cdots z_{k,M}]^T. \tag{6}$$

The stacked TDOA measurement z_k is denoted as

$$z_k = h(e_k) + v_k, \tag{7}$$
$$h(e_k) = [h_2(e_k) \; h_3(e_k) \; \cdots \; h_M(e_k)]^T, \tag{8}$$
$$v_k = [v_{k,2} \; v_{k,3} \; \cdots \; v_{k,M}]^T, \tag{9}$$

where $v_k \sim \mathcal{N}(0, R_k)$ and R_k is the measurement error covariance matrix.

Since all TDOA measurements are generated under a common reference sensor, the measurement noises are mutually correlated and the off-diagonal entries of the corresponding

covariance matrix become non-zero values [18]. The measurement error covariance matrix $\boldsymbol{R}_k$ is denoted as

$$\boldsymbol{R}_k = E[\boldsymbol{v}_k \boldsymbol{v}_k^T] = \begin{bmatrix} \sigma_{1,2}^2 & \sigma_1^2 & \cdots & \sigma_1^2 \\ \sigma_1^2 & \sigma_{1,3}^2 & \cdots & \sigma_1^2 \\ \vdots & \vdots & \ddots & \vdots \\ \sigma_1^2 & \sigma_1^2 & \cdots & \sigma_{1,M}^2 \end{bmatrix}. \quad (10)$$

Given that the sensor network is homogeneous, i.e., the standard deviation of sensor noise is equal to σ_u, then eq (10) becomes

$$\boldsymbol{R}_k = 2\sigma_u^2 \begin{bmatrix} 1 & 0.5 & \cdots & 0.5 \\ 0.5 & 1 & \cdots & 0.5 \\ \vdots & \vdots & \ddots & \vdots \\ 0.5 & 0.5 & \cdots & 1 \end{bmatrix} \triangleq 2\sigma_u^2 \boldsymbol{\Phi}_k, \quad (11)$$

where matrix $\boldsymbol{\Phi}_k$ is further utilized for the TDOA measurement decorrelation in Section III.

III. TDOA NOISE DECORRELATION

The standard EKF update for a stacked measurement vector $\boldsymbol{z}_k$ is performed simultaneously with the entire measurement vector, which is called the parallel update. If the measurement noises are uncorrelated, then the measurement error covariance matrix is diagonal and one can perform the EKF update sequentially with one component of the measurement vector at a time, which is called serial update.

In TDOA-based tracking systems, the measurement noises are correlated and the corresponding covariance matrix $\boldsymbol{R}_k$ is not diagonal such that the serial update cannot be directly applied. Since $\boldsymbol{R}_k$ is a positive-definite matrix, one can apply a linear transformation to diagonalize it. An efficient technique to achieve the diagonalization is through the Cholesky decomposition [20] and yields

$$\boldsymbol{R}_k = \boldsymbol{D}_k \boldsymbol{\Lambda}_k \boldsymbol{D}_k^T, \quad (12)$$

where $\boldsymbol{D}_k$ is a unit lower triangular matrix, $\boldsymbol{\Lambda}_k = 2\sigma_u^2 \boldsymbol{I}_{M-1}$ and $\boldsymbol{I}_n$ denotes an $n \times n$ identity matrix.

Denote the (m, n)th entries in $\boldsymbol{\Phi}_k$ and $\boldsymbol{D}_k$ as $\boldsymbol{\Phi}_k^{m,n}$ and $\boldsymbol{D}_k^{m,n}$, respectively. The decomposition matrix $\boldsymbol{D}_k$ is

$$\boldsymbol{D}_k = \begin{bmatrix} \boldsymbol{D}_k^{1,1} & 0 & \cdots & 0 \\ \boldsymbol{D}_k^{2,1} & \boldsymbol{D}_k^{2,2} & \cdots & 0 \\ \vdots & \vdots & \ddots & \vdots \\ \boldsymbol{D}_k^{M-1,1} & \boldsymbol{D}_k^{M-1,2} & \cdots & \boldsymbol{D}_k^{M-1,M-1} \end{bmatrix}, \quad (13)$$

and its entries are given by

$$\boldsymbol{D}_k^{m,n} = \begin{cases} \sqrt{\boldsymbol{\Phi}_k^{m,n} - \sum_{j=1}^{n-1} (\boldsymbol{D}_k^{n,j})^2}, & m = n; \\ \left(\boldsymbol{\Phi}_k^{m,n} - \sum_{j=1}^{n-1} \boldsymbol{D}_k^{m,j} \boldsymbol{D}_k^{n,j}\right) / \boldsymbol{D}_k^{n,n}, & m > n; \\ 0, & otherwise. \end{cases}$$

Denote the stacked sensor noise in range domain as $\boldsymbol{g}_k = [cu_{k,2}, \cdots, cu_{k,M}]^T$. The covariance of uncorrelated measurement noise is defined by $\boldsymbol{\Lambda}_k = E[\boldsymbol{g}_k \boldsymbol{g}_k^T]$.

Consequently, the covariance matrix $\boldsymbol{R}_k$ can be presented in the form

$$\boldsymbol{R}_k = \boldsymbol{D}_k E[\boldsymbol{g}_k \boldsymbol{g}_k^T] \boldsymbol{D}_k^T = E[\boldsymbol{D}_k \boldsymbol{g}_k \boldsymbol{g}_k^T \boldsymbol{D}_k^T], \quad (14)$$

as the entries in $\boldsymbol{D}_k$ are constants determined by the sensor network. Together with (10) yields

$$\boldsymbol{v}_k = \boldsymbol{D}_k \boldsymbol{g}_k. \quad (15)$$

The stacked TDOA measurement vector $\boldsymbol{z}_k$ in (7) can be rewritten as

$$\boldsymbol{z}_k = \boldsymbol{h}(\boldsymbol{e}_k) + \boldsymbol{D}_k \boldsymbol{g}_k. \quad (16)$$

Multiplying both sides with $\boldsymbol{D}_k^{-1}$, one can use the transformed pseudo-measurement vector $\boldsymbol{z}_k^p$ instead of $\boldsymbol{z}_k$:

$$\boldsymbol{z}_k^p = \boldsymbol{D}_k^{-1} \boldsymbol{z}_k \quad (17)$$
$$= \boldsymbol{D}_k^{-1} \boldsymbol{h}(\boldsymbol{e}_k) + \boldsymbol{g}_k, \quad (18)$$

where $\boldsymbol{g}_k$ is the pseudo-measurement noise vector which follows

$$\boldsymbol{g}_k \sim \sqrt{2} \begin{bmatrix} \mathcal{N}(0, \sigma_u) \\ \mathcal{N}(0, \sigma_u) \\ \vdots \\ \mathcal{N}(0, \sigma_u) \end{bmatrix}. \quad (19)$$

The covariance matrix of $\boldsymbol{g}_k$ is equivalent to $\boldsymbol{\Lambda}_k$, which is diagonal, and the pseudo-measurement $\boldsymbol{z}_k^p$ is uncorrelated. Consequently the uncorrelatedness of pseudo-measurement noises guarantees the use of EKF serial update.

The Jacobian matrix of the measurement function $\boldsymbol{h}(\boldsymbol{e}_k)$ is given by

$$\boldsymbol{H}_k = \frac{\partial \boldsymbol{h}(\boldsymbol{e}_k)}{\partial \boldsymbol{e}_k}. \quad (20)$$

Similarly, instead of $\boldsymbol{H}_k$, one can utilize the pseudo Jacobian matrix given by

$$\boldsymbol{H}_k^p = \boldsymbol{D}_k^{-1} \boldsymbol{H}_k. \quad (21)$$

IV. TRACKING WITH DECORRELATED TDOA MEASUREMENTS

In this section, both the EKF parallel update and the EKF serial update with decorrelated TDOA measurements are described for comparative analysis. The startup of EKF requires an informative prior state estimate and covariance such that the TDOA measurements received at the first scan are utilized for track initialization. The track state is recursively propagated via the EKF prediction step and corrected by the received measurements in the EKF update step. A flowchart of the tracking procedure is illustrated in Fig. 3.

A. TRACK INITIALIZATION

The least square (LS) approach has been widely studied in TDOA measurement-based target localization [22], [23]. The method in [22] provides a simple but efficient solution by neglecting the quadratic constraint. Reference [23] improves
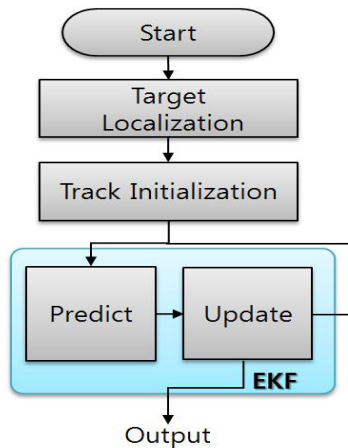
FIGURE 3. Flowchart of target tracking.

the localization accuracy by introducing a Lagrange multiplier and the solution is obtained through a bisection algorithm, which makes it computationally expensive. Although the solution in [22] is not as accurate as the one in [23], it requires fewer computations and its inaccuracy can be compensated by the EKF update in the next few scans. Therefore the method in [22] is adopted in this paper for track initialization. The localized target position $\begin{bmatrix} \hat{x}_0 & \hat{y}_0 & \hat{z}_0 \end{bmatrix}^T$ is used as the initial state estimate in one-point track initialization [24]. The initial track is parameterized by an initial state estimate e_0 and an initial covariance matrix P_0 that are given by

$$e_0 = \begin{bmatrix} \hat{x}_0 & \hat{y}_0 & \hat{z}_0 & 0 & 0 & 0 \end{bmatrix}^T, \qquad (22)$$

$$P_0 = \begin{bmatrix} 0.5^2 I_3 & 0_3 \\ 0_3 & v_{max}^2 I_3/3 \end{bmatrix}, \qquad (23)$$

where v_{max} is the maximum target velocity determined by the designers.

B. EKF PARALLEL UPDATE

In the EKF parallel update, the track state is updated simultaneously with the entire measurement vector z_k. Consequently parameters in EKF such as the Jacobian matrix H_k, the filter gain matrix K_k, the predicted measurement error covariance matrix S_k and the predicted measurement vector z_k have to be augmented into stacked form. This lead to difficulties in implementing the filter in practice.

Denote the predicted mean and covariance of track state as $\bar{e}_k$ and covariance $\bar{P}_k$, respectively. The standard EKF parallel update formulae are given by

$$\hat{e}_k = \bar{e}_k + K_k \left(z_k - h(\bar{e}_k) \right), \qquad (24)$$

$$\hat{P}_k = \bar{P}_k - K_k H_k \bar{P}_k, \qquad (25)$$

where $\hat{e}_k$ and $\hat{P}_k$ are the posterior mean and covariance matrix with

$$K_k = \bar{P}_k H_k^T S_k^{-1}, \qquad (26)$$

$$S_k = H_k \bar{P}_k H_k^T + R_k. \qquad (27)$$

The dimensions of K_k and S_k are $6 \times (M - 1)$ and $(M - 1) \times (M - 1)$, respectively.

C. EKF SERIAL UPDATE

Compared to the parallel update, the serial update uses measurements from different sensors sequentially instead of handling the entire measurement vector all at once, enabling a tracking system to execute complicated tasks by utilizing free time for several easier subtasks.

The subtasks should be executed iteratively within one sampling interval. In the m-th iteration of serial update, the pseudo Jacobian matrix, the pseudo measurement and the predicted measurement are denoted as $H_{k,m}^p$, $z_{k,m}^p$ and $\bar{z}_{k,m}$, respectively. The (m, n)th entry in D_k^{-1} is denoted as $D_k^{-1}(m, n)$. The ith row in H_k is denoted as $H_{k,i}$. According to (21), the pseudo Jacobian matrix $H_{k,m}^p$ is calculated by a linear combination of the entries in D_k^{-1} and H_k such that

$$H_{k,m}^p = \sum_{i=1}^m D_k^{-1}(m, i) H_{k,i} \qquad (28)$$

The noise decorrelation process is executed iteratively instead of implementing all matrix operations, as in eq (21). Meanwhile, less storage is required as $H_{k,m}^p$ is the mth row in H_k^p. Similar calculations are also applied to obtain $z_{k,m}^p$ and $\bar{z}_{k,m}$.

The posterior mean and covariance of the track state at iteration m are denoted as $\hat{e}_{k,m}$ and covariance $\hat{P}_{k,m}$, which are used as inputs of the next iteration until the exhaustiveness of pseudo-measurements. Algorithm 1 is the pseudo-code of the EKF serial update. The matrix dimensions of K_k and S_k have been reduced to 6×1 and 1×1 compared to the ones in parallel update.

Algorithm 1 Serial EKF Update

1: **for** $m = 1 : M - 1$ **do**
2: $\quad H_{k,m}^p = [0\,0\,0\,0\,0\,0]$, $\bar{z}_{k,m} = 0$, $z_{k,m}^p = 0$
3: $\quad$ **for** $n = 1 : m$ **do**
4: $\quad\quad H_{k,n} = \frac{\partial h_n(e_k)}{\partial e_k}|_{e_k = \bar{e}_k}$
5: $\quad\quad H_{k,m}^p = H_{k,m}^p + D_k^{-1}(m, n) H_{k,n}$
6: $\quad\quad \bar{z}_{k,m} = \bar{z}_{k,m} + D_k^{-1}(m, n) h_n(\bar{e}_k)$
7: $\quad\quad z_{k,m}^p = z_{k,m}^p + D_k^{-1}(m, n) z_{k,n}$
8: $\quad$ **end for**
9: $\quad S_{k,m} = H_{k,m}^p \bar{P}_k (H_{k,m}^p)^T + 2\sigma_u^2$
10: $\quad K_{k,m} = \bar{P}_k (H_{k,m}^p)^T S_{k,m}^{-1}$
11: $\quad \hat{e}_{k,m} = \bar{e}_k + K_{k,m} \left(z_{k,m}^p - \bar{z}_{k,m} \right)$
12: $\quad \hat{P}_{k,m} = \bar{P}_k - K_{k,m} H_{k,m}^p \bar{P}_k$
13: $\quad \bar{e}_k = \hat{e}_{k,m}$
14: $\quad \bar{P}_k = \hat{P}_{k,m}$
15: **end for**

Intuitively the application of the Cholesky decomposition may induce additional matrix inverse operations of D_k since $D_k^{-1}(m, n)$ is involved in every iteration, but this additional computation can be significantly reduced by precomputation

of the matrix. The inverse of Cholesky decomposition matrix $\boldsymbol{D}_k$ depends only on the sensor number M such that its entries become invariant once the sensor network is determined. Therefore, the entries $\boldsymbol{D}_k^{-1}(m, n)$ can be precomputed off-line and stored in the dataset. The relevant value of $\boldsymbol{D}_k^{-1}(m, n)$ can be utilized immediately from the dataset instead of being calculated repeatedly, and the algorithmic efficiency is increased substantially.

Note that if N_{md} sensors fail to receive the UWB signals, then the iteration number in Algorithm 1 changes to $M - 1 - N_{md}$. For situations where $M - 1 - N_{md}$ is less than 3, the target state observability cannot be satisfied in 3-dimensional scenarios, the updated track state will be given by the predicted track state, namely $\hat{\boldsymbol{e}}_k = \bar{\boldsymbol{e}}_k$ and $\hat{\boldsymbol{P}}_k = \bar{\boldsymbol{P}}_k$.

D. COMPUTATIONAL ANALYSIS

Although evaluation metrics of indoor target localization systems vary in different applications, the computational load should always be addressed. The localization result is used as an input for the subsequent control systems such that an accurate and rapid result is required. The computational complexity of a filter is analyzed by giving the number of floating-point operations (flops) in this paper. A flop is a measure of counting computations, including addition/subtraction and multiplication/division between two floating-point numbers. The equivalent flop (EF) complexity is proposed in [25] to reflect the flop complexity of the matrix and vector operations. The prediction EF complexity for the parallel update is identical to the serial update while the update EF complexities are different.

The EF complexities of the parallel update and the serial update are given by

$$C_{parallel}(M) = M^3 + 21M^2 + 232M - 254 + (M - 1)d_1,$$
(29)

$$C_{serial}(M) = 8M^2 + 336M - 344 + \frac{(M - 1)M}{2}d_1,$$
(30)

where d_1 is the EF complexity of linearization of the predicted state. Note that $M \geqslant 2$ as the TDOA measurement cannot be generated by only one sensor. For the case of $M = 1$, no TDOA measurement is generated and the tracking system fails to update the track state with received measurements, then the relevant EF complexities become $C_{parallel}(1) = C_{serial}(1) = 0$.

Details of the EF complexity for each update scheme are shown in Tables 1 and 2. For example, the first instruction $\bar{\boldsymbol{P}}_k \boldsymbol{H}_k^T$ in Table 1 corresponds to multiply $\bar{\boldsymbol{P}}_k \in \mathbb{R}^{6 \times 6}$ with $\boldsymbol{H}_k^T \in \mathbb{R}^{6 \times (M-1)}$, which requires $6^2(M - 1)$ multiplications and $6 \cdot 5(M - 1)$ additions. The first instruction $\boldsymbol{H}_{k,m}^p = \boldsymbol{H}_{k,m}^p + \boldsymbol{D}_k^{-1}(m, n)\boldsymbol{H}_{k,n}$ in Table 2 corresponds to multiply $\boldsymbol{D}_k^{-1}(m, n) \in \mathbb{R}^{1 \times 1}$ with $\boldsymbol{H}_{k,n} \in \mathbb{R}^{1 \times 6}$ and plus with $\boldsymbol{H}_{k,m}^p \in \mathbb{R}^{1 \times 6}$, which requires 6 multiplications and 6 additions. This instruction is repeated m times in the m-th iteration as shown in Algorithm 1. The sum of repeated time for this instruction up to the m-th iteration is $m(m+1)/2$.

Therefore, $6 \cdot (M - 1)M/2$ multiplications as well as additions are executed when there exists $M - 1$ TDOA measurements.

The characteristic curves of $C_{parallel}(M)$ and $C_{serial}(M)$ with regard to the sensor number M are shown in Fig. 4. The serial update has an EF complexity close to the one of the parallel update when $M \leqslant 5$, and exhibits a significant reduction in EF complexity when $M > 5$. Such superiority becomes more obvious as the number of sensors increases, making the serial update more appropriate for situations where large scale sensors are required.
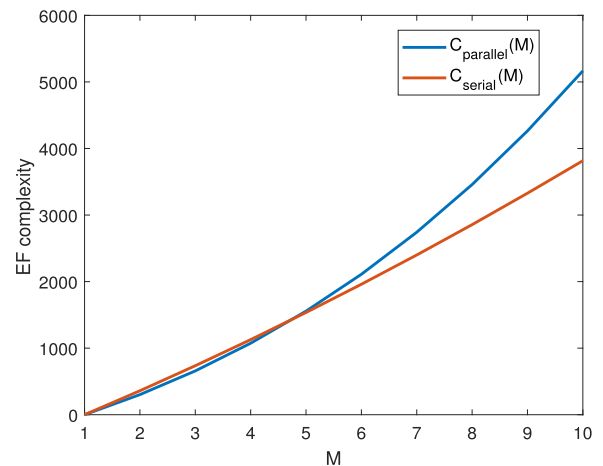

FIGURE 4. EF complexities of parallel update and serial update.

The serial update utilizes the measurement from one sensor at a time that the computations in one iteration can be significantly reduced since high dimensional matrix operations are avoided. The iteration number can be flexibly adjusted so that there exists a trade-off between the tracking performance and computational requirements as long as the target observability is satisfied, i.e., the iteration number should be at least 3.

V. SIMULATION

In this section numerical results for a three-dimensional tracking scenario are presented, in which $M = 8$ homogeneous sensors (standard deviation of sensor noise in range domain $\sigma_u = 0.3$ m) are deployed at two different layers (5 m and 15 m above the ground) and passively receive signals emitted from the target with a frequency of $f_0 = 30$ Hz. Sensor s_1 is set as the reference sensor for TDOA measurement generation.

For target tracking using TDOA only measurements, the tracking accuracy depends on sensor-target geometry such that evaluations for sensor deployment are necessary. The Cramer-Rao lower bound (CRLB), which indicates the best theoretical performance of filters by the root mean squared error (RMSE), is used in this simulation as evaluation criterion for sensor deployment. The CRLB at every point in $x - y$ plane is calculated by [26]

$$CRLB = \sqrt{\boldsymbol{J}^{-1}(1, 1) + \boldsymbol{J}^{-1}(2, 2) + \boldsymbol{J}^{-1}(3, 3)},$$
(31)

TABLE 1. EF complexity for the EKF parallel update in Section IV-B.

Instruction	Multi.	Add.	Others
$T_1 = \bar{\boldsymbol{P}}_k \boldsymbol{H}_k^T$	$6^2 \cdot (M-1)$	$6 \cdot 5(M-1)$	
$\boldsymbol{S}_k = \boldsymbol{H}_k T_1 + \boldsymbol{R}_k$	$6(M-1)^2$	$5(M-1)^2 + (M-1)^2$	
$inv\boldsymbol{S}_k = \boldsymbol{S}_k^{-1}$			$(M-1)^3$
$T_2 = \boldsymbol{H}_k^T inv\boldsymbol{S}_k$	$6(M-1)^2$	$6(M-1)(M-2)$	
$\boldsymbol{K}_k = \bar{\boldsymbol{P}}_k T_2$	$6^2 \cdot (M-1)$	$6 \cdot 5(M-1)$	
$T_3 = h(\bar{\boldsymbol{e}}_k)$			$(M-1)d_1$
$\tilde{\boldsymbol{z}}_k = \boldsymbol{z}_k - h(\bar{\boldsymbol{e}}_k)$		$M-1$	
$T_4 = \boldsymbol{K}_k \tilde{\boldsymbol{z}}_k$	$6(M-1)$	$6(M-2)$	
$\hat{\boldsymbol{e}}_k = \bar{\boldsymbol{e}}_k + T_4$		6	
$T_5 = \boldsymbol{H}_k \bar{\boldsymbol{P}}_k$	$6^2 \cdot (M-1)$	$6 \cdot 5(M-1)$	
$\hat{\boldsymbol{P}}_k = \bar{\boldsymbol{P}}_k - \boldsymbol{K}_k T_5$	$6^2 \cdot (M-1)$	$6^2 \cdot (M-2) + 6^2$	

TABLE 2. EF complexity for the EKF serial update in Algorithm 1.

Instruction	Multi.	Add.	Others
$\boldsymbol{H}_{k,m}^p = \boldsymbol{H}_{k,m}^p + \boldsymbol{D}_k^{-1}(m,n)\boldsymbol{H}_{k,n}$	$6 \cdot \frac{(M-1)M}{2}$	$6 \cdot \frac{(M-1)M}{2}$	
$T_1 = h_n(\bar{\boldsymbol{e}}_k)$			$d_1 \cdot \frac{(M-1)M}{2}$
$\bar{\boldsymbol{z}}_{k,m} = \bar{\boldsymbol{z}}_{k,m} + \boldsymbol{D}_k^{-1}(m,n)T_1$	$\frac{(M-1)M}{2}$	$\frac{(M-1)M}{2}$	
$\boldsymbol{z}_{k,m}^p = \boldsymbol{z}_{k,m}^p + \boldsymbol{D}_k^{-1}(m,n)\boldsymbol{z}_{k,n}$	$\frac{(M-1)M}{2}$	$\frac{(M-1)M}{2}$	
$T_2 = \bar{\boldsymbol{P}}_k (\boldsymbol{H}_{k,m}^p)^T$	$6^2(M-1)$	$6 \cdot 5(M-1)$	
$\boldsymbol{S}_{k,m} = \boldsymbol{H}_{k,m}^p T_2 + 2\sigma_u^2$	$6(M-1)$	$5(M-1) + (M-1)$	
$inv\boldsymbol{S}_{k,m} = \boldsymbol{S}_{k,m}^{-1}$			$(M-1)$
$T_3 = (\boldsymbol{H}_{k,m}^p)^T inv\boldsymbol{S}_{k,m}$	$6(M-1)$		
$\boldsymbol{K}_{k,m} = \bar{\boldsymbol{P}}_k T_3$	$6^2 \cdot (M-1)$	$6 \cdot 5(M-1)$	
$\tilde{\boldsymbol{z}}_{k,m} = \boldsymbol{z}_{k,m}^p - \bar{\boldsymbol{z}}_{k,m}$		$M-1$	
$T_4 = \boldsymbol{K}_{k,m} \tilde{\boldsymbol{z}}_{k,m}$	$6(M-1)$		
$\hat{\boldsymbol{e}}_{k,m} = \bar{\boldsymbol{e}}_k + T_4$		$6(M-1)$	
$T_5 = \boldsymbol{H}_{k,m}^p \bar{\boldsymbol{P}}_k$	$6^2 \cdot (M-1)$	$6 \cdot 5(M-1)$	
$\hat{\boldsymbol{P}}_{k,m} = \bar{\boldsymbol{P}}_k - \boldsymbol{K}_{k,m} T_5$	$6^2 \cdot (M-1)$	$6^2 \cdot (M-1)$	
$\bar{\boldsymbol{e}}_k = \hat{\boldsymbol{e}}_{k,m}$		$6(M-1)$	
$\bar{\boldsymbol{P}}_k = \hat{\boldsymbol{P}}_{k,m}$		$6^2 \cdot (M-1)$	

where $\boldsymbol{J}^{-1}(i,j)$ indicates the (i,j)th entry in the inverse of the Fisher information matrix $\boldsymbol{J}$, where

$$\boldsymbol{J} = \boldsymbol{H}_k^T \boldsymbol{R}_k^{-1} \boldsymbol{H}_k. \tag{32}$$

A collection of all CRLB values in the $x-y$ plane forms a CRLB distribution, as illustrated in Fig. 6, where the CRLB values are quantized and distinguished by a color bar on the right side. As shown in Fig. 6, most of the surveillance region is shaded in blue, showing that the theoretical estimation error is small and the sensors are deployed appropriately.

In the simulation, both the correlated and the uncorrelated TDOA measurement error covariance matrices are used for the EKF parallel update to investigate the influence of the measurement noise correlation. To verify the effectiveness of the proposed approach, we simulate both the EKF parallel updates with both the correlated and the uncorrelated measurements, and the EKF serial update with the decorrelated TDOA measurements. The corresponding simulation
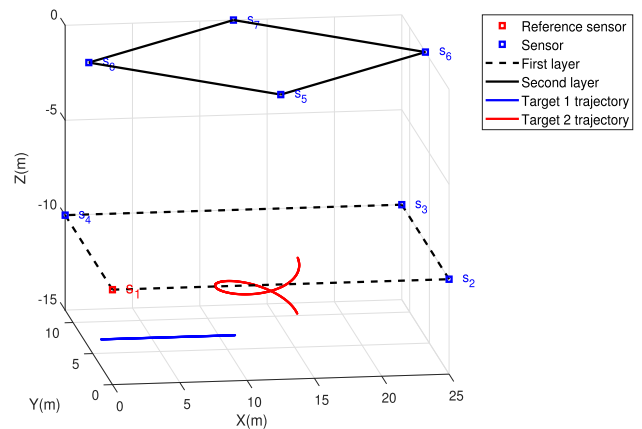

FIGURE 5. An example of target to sensors geometry in the UWB target tracking system.

results are denoted as EKF parallel(differentiated by marks of correlated noise and uncorrelated noise) and D-EKF serial, respectively. The simulation tests with 200 Monte Carlo runs

TABLE 3. Execution time for one sampling interval ($T_s = 1/f_0 \approx 33.3\ ms$).

Method	Parallel(correlated noise)	Parallel(uncorrelated noise)	Serial
Time (ms)	3.129	2.936	0.651

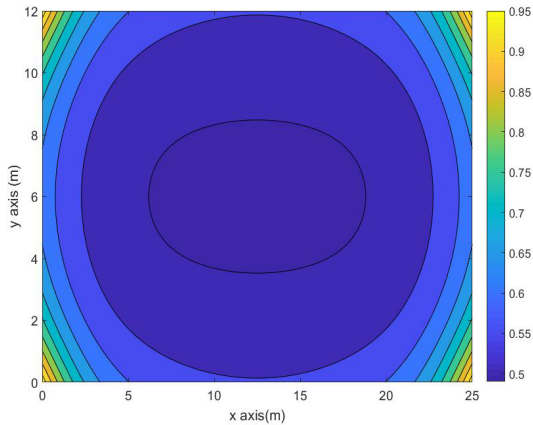**FIGURE 6.** CRLB of the TDOA scenario.

FIGURE 7. RMSE comparisons for (a) target 1 (b) target 2.

and the simulation scenario time for each run is 20 s. Target 1 starts from an initial position $[0,\ 3,\ -13.6]^T$ m and moves with the constant velocity $[0.5,\ 0,\ 0]^T$ m/s. Target 2 starts from an initial position $[12.5,\ 6,\ -13.6]^T$ m. Target 2 follows the dynamics of circular motion in $x - y$ plane with constant angular velocity 0.314 rad/s and radius 3 m, and follows rectilinear motion in z axis with constant velocity 0.15 m/s. The target trajectories for both targets are depicted in Fig. 5.

The transition matrix and process noise covariance matrix for all EKFs are given by

$$\boldsymbol{F}_k = \boldsymbol{I}_3 \otimes \begin{bmatrix} 1 & T_s \\ 0 & 1 \end{bmatrix}, \quad \boldsymbol{Q}_k = \boldsymbol{I}_3 \otimes \sigma_\omega^2 \begin{bmatrix} \dfrac{T_s^4}{4} & \dfrac{T_s^3}{2} \\ \dfrac{T_s^3}{2} & T_s^2 \end{bmatrix}, \quad (33)$$

where $T_s = 1/f_0$ is the sampling time, $\otimes$ denotes the Kronecker product and the standard deviation of the process noise is $\sigma_\omega = 0.707$ m/s^2. Although the transition matrix in (33) does not coincide with the dynamics of target 2, this can be compensated by a high sampling frequency. According to the beacon-enabled slotted MAC protocol discussed in Section II-A, measurement origins are known to the UWB tracking system and measurement-to-track data association are not involved. The received measurements are divided into different groups based on the attached target ID number. The EKFs are applied separately to track the corresponding target. The tracking performance is evaluated by RMSE, which indicates the accuracy of the estimated target trajectory.

The RMSE curves in Fig. 7 show that the EKF parallel update with the correlated covariance matrix delivers smaller RMSE relative to the one with the uncorrelated covariance matrix, which demonstrates the necessity of considering TDOA noise correlation. The several peaks in Fig. 7(b) can
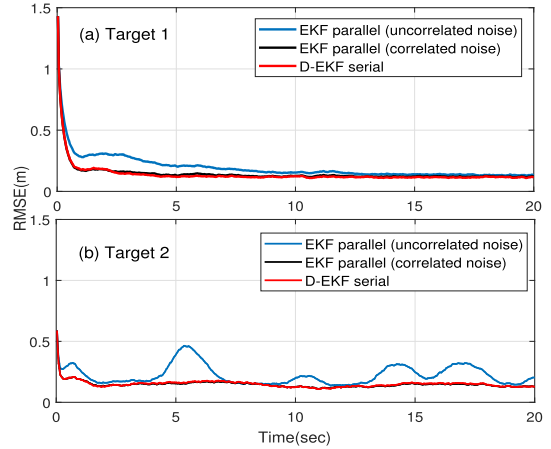
be attributed to a mismatch between the real measurement uncertainty coverage and the estimated one [11]. When the target performs a circular motion in $x - y$ plane, the coverage of TDOA measurement uncertainty rotates along with the target movement. Neglecting the measurement noise correlation in the EKF parallel update with uncorrelated covariance matrix makes the filter fail to adjust its predicted covariance according to the target movement, which leads to the tracking performance deterioration.

The D-EKF serial update has similar estimation errors to the EKF parallel update (correlated noise). The inequality in tracking performance can be attributed to different linearization errors in the Jacobian matrix calculations. The Jacobian matrix in parallel update is calculated simultaneously by differentiating w.r.t the predicted state $\bar{\boldsymbol{e}}_k$, whereas the Jacobian matrix of the serial update is replaced by a pseudo Jacobian matrix and the differentiated $\bar{\boldsymbol{e}}_k$ varies in each iteration. Both update schemes deliver an averaged RMSE around 0.15 m, which suggests the TDOA measurement noise ($\sqrt{2}\sigma_u \approx 0.42$ m) is filtered effectively.

The simulation is conducted on a Windows 7 operating system (Intel i7-6700 CPU, 16.0 GB RAM) and run using the MATLAB program. Table 3 lists the execution time for both schemes. The serial update scheme outperforms the parallel update scheme as the execution time is significantly reduced. The larger matrix dimensions in parallel update lead to more matrix computations.

VI. EXPERIMENTAL RESULTS

This section presents the experimental results obtained from applying the proposed algorithm to the UWB real-time localization system (UWB-RTLS). The experiment is conducted
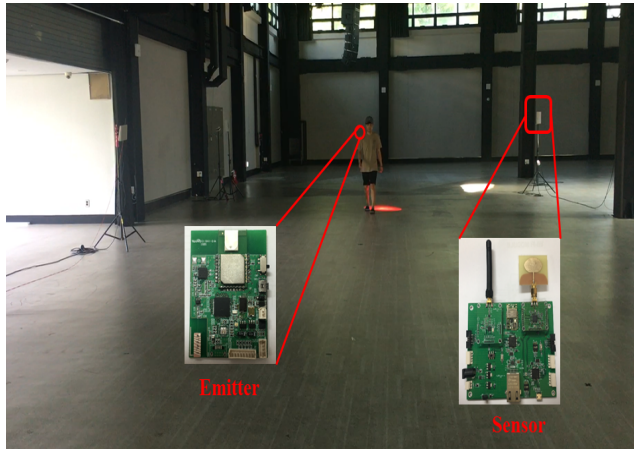
FIGURE 8. The UWB-RTLS tracking experiment scenario.

in an indoor environment where one active emitter is mounted on a moving person and 8 passive sensors are deployed at designated positions as shown in Fig. 8. The sensor-target geometry is similar to the one in Section V.

The UWB-RTLS is implemented via the C language on a micro-controller STM32F105RCT6, which is implemented as a host micro-controller to Decawave's DW1000 UWB chips. The DW1000 is an IEEE 802.15.4 compliant transceiver for wireless sensor networks and real-time localization systems. The chip builds on the advantages of ultra-wideband, such as unlicensed operation, robustness in multi-path environments, high precision ranging and low power transmission. The UWB radio signal is emitted periodically from the target to the stationary sensors and each sensor sends its timestamp of the received signals to the fusion center.

For practical implementations of the UWB-RTLS, clock synchronization between the reference sensor and the other sensors is critical, as it affects the tracking performance significantly. In this experiment, a Kalman filter is applied to improve the clock synchronization [19] and the experiment results are shown in Fig. 9. The skew ratio of the measured clock relative to the reference clock and the clock offset are estimated so that the two clocks are synchronized by the Kalman filter [19]. The fluctuation of the original measured data indicates the instability of clock synchronization, and this phenomenon disappears after applying the Kalman filter.

The person carrying the emitter follows predetermined routes with a relatively constant velocity. The corresponding parameters are adjusted to the motion of the human (e.g., maximum velocity v_{max}, and standard deviation of process noise σ_ω) and sensor characteristics (e.g., standard deviation of sensor noise σ_u). Several maneuvers are designed to test the robustness of the proposed algorithm. To enable the UWB-RTLS operate in real time, a trade-off between the tracking performance and computational load is made. The interactive multiple model (IMM) algorithm [20], which aims to handle the target maneuvering problem with higher
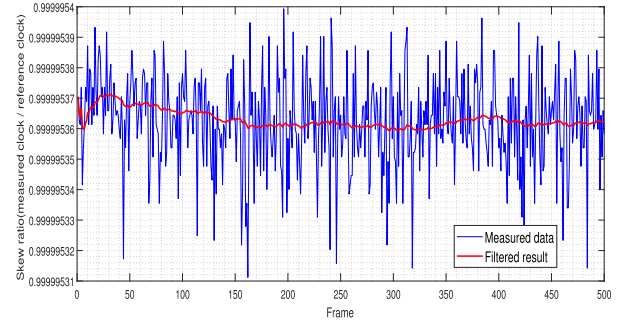

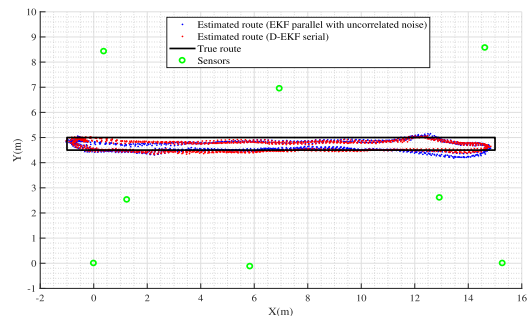**FIGURE 9.** Clock synchronization by Kalman filter.

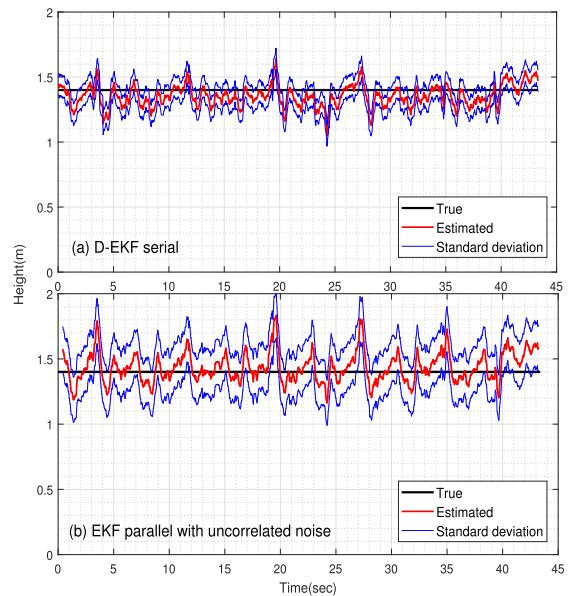**FIGURE 10.** Ground truth route and estimated route.

FIGURE 11. Statistics of target height for: (a) D-EKF serial (b) EKF parallel with uncorrelated noise.

computational cost, is not adopted in this experiment. The filter has only one target dynamical model as denoted in (33), so the tracking performance is expected to degrade when the target maneuvers. The tracking performance degradation can be compensated as the high sampling frequency condition provides more target information within a fixed time.

In this experiment, the target moves in horizontal plane while the target height is kept constant. The vertical view

of the experiment scenario is illustrated in Fig. 10. The performance of D-EKF is compared with that of the EKF parallel update with the uncorrelated covariance matrix in this experiment. As can be seen in Fig. 10, precise estimation can be achieved when the target moves towards one direction. The estimation accuracy degrades slightly when the target takes a turn (90 degree maneuver) but recovers quickly. The estimated target height and the relevant statistics are depicted in Fig. 11. Since the target height remains time-invariant, all estimated heights over the entire experiment can be used to calculate the corresponding mean value and standard deviation. The mean value of target height in Fig. 11(a) is 1.35 m which is very close to the true value 1.4 m. The corresponding standard deviation value is 0.08 m, which suggests good stability of the estimation results. Contrastively the EKF parallel update with uncorrelated noise in Fig. 11(b) shows severe fluctuations with standard deviation value 0.17 m.

VII. CONCLUSION

This paper presents a modified EKF serial update, which replaces the standard Jacobian matrix and measurement vector with pseudo versions, for indoor target tracking using TDOA measurements with applications to ultra-wideband systems. TDOA measurement shows a high accuracy due to the large bandwidth UWB signals, but its application is constrained by the correlated measurement noise. The proposed method releases the constraint by applying the Cholesky decomposition to convert the correlated TDOA noise into a mathematically equivalent and uncorrelated pseudo-noise. Therefore the decomposition matrix can be integrated naturally with the EKF serial update, and fusing the TDOA measurements from multiple sensors can be achieved without information loss. Other advantages of the serial update include the lower-dimensional matrix operations and lower storage requirements relative to the parallel update, which is validated by theoretical analyses and simulation studies in this paper. The experimental results demonstrate the accuracy of the tracking results and the ability of handling target maneuvers.

REFERENCES

[1] J. Luo, Z. Zhang, C. Liu, and H. Luo, "Reliable and cooperative target tracking based on WSN and WiFi in indoor wireless networks," *IEEE Access*, vol. 6, pp. 24846–24855, 2018.

[2] J. D. Taylor, *Introduction to Ultra-Wideband Radar Systems*. Boca Raton, FL, USA: CRC Press, 1994.

[3] A. Eryildirim and M. B. Guldogan, "A Gaussian mixture Bernoulli filter for extended target tracking with application to an ultra-wideband localization system," *Digit. Signal Process.*, vol. 57, pp. 1–12, Oct. 2016.

[4] A. Alari, A. Al-Salman, M. Alsaleh, A. Alnafessah, S. Al-Hadhrami, M. A. Al-Ammar, and H. S. Al-Khalifa, "Ultra wideband indoor positioning technologies: Analysis and recent advances," *Sensors*, vol. 16, no. 5, pp. 707–742, 2016.

[5] Z. Sahinoglu, S. Gezici, and I. Güvenc, *Ultra-wideband Positioning Systems: Theoretical Limits, Ranging Algorithms, and Protocols*. Cambridge, U.K.: Cambridge Univ. Press, 2008.

[6] M. McCracken, M. Bocca, and N. Patwari, "Joint ultra-wideband and signal strength-based through-building tracking for tactical operations," in *Proc. 10th Annu. IEEE Int. Conf. Sens., Commun. Netw. (SECON)*, Jun. 2013, pp. 309–317.

[7] M. Tuchler, V. Schwarz, and A. Huber, "Location accuracy of an UWB localization system in a multi-path environment," in *Proc. IEEE Int. Conf. Ultra-Wideband (ICU)*, Sep. 2005, pp. 414–419.

[8] H. R. Hashemipour, S. Roy, and A. J. Laub, "Decentralized structures for parallel Kalman filtering," *IEEE Trans. Autom. Control*, vol. AC-33, no. 1, pp. 88–94, Jan. 1988.

[9] H. You, L. Dajin, and P. Yingning, "State estimation for multilevel multisensor data fusion systems," *Acta Electron. Sinica*, vol. 8, pp. 8–16, Aug. 1999.

[10] Q. Gan and C. J. Harris, "Comparison of two measurement fusion methods for Kalman-filter-based multisensor data fusion," *IEEE Trans. Aerosp. Electron. Syst.*, vol. 37, no. 1, pp. 273–279, Jan. 2001.

[11] Y. Xie, J. H. Lee, and T. L. Song, "Analysis for reference sensor selection in time difference of arrival-based localisation," *IET Electron. Lett.*, vol. 54, no. 25, pp. 1454–1456, 2018.

[12] Y. Bar-Shalom, P. K. Willett, and X. Tian, *Tracking and Data Fusion: A Handbook of Algorithms*. Bradford, U.K.: YBS, 2011.

[13] L. Y. Pao and C. W. Frei, "A comparison of parallel and sequential implementations of a multisensor multitarget tracking algorithm," in *Proc. Amer. Control Conf.*, 1995, pp. 1683–1687.

[14] L. Y. Pao and L. Trailovic, "The optimal order of processing sensor information in sequential multisensor fusion algorithms," *IEEE Trans. Autom. Control*, vol. 45, no. 8, pp. 1532–1536, Aug. 2000.

[15] Y. Xie, H. Lee, M. Ahn, B. J. Lee, and T. L. Song, "Joint integrated track splitting for multi-sensor multi-target tracking in clutter," in *Proc. 13th Int. Conf. Inform. Control, Automat. Robot.*, 2016, pp. 299–307.

[16] Z. Duan, X. R. Li, C. Han, and H. Zhu, "Sequential unscented Kalman filter for radar target tracking with range rate measurements," in *Proc. 8th Int. Conf. Inf. Fusion*, 2005, pp. 8–15.

[17] K. C. Ho and Y. T. Chan, "Solution and performance analysis of geolocation by TDOA," *IEEE Trans. Aerosp. Electron. Syst.*, vol. 29, no. 4, pp. 1311–1322, Oct. 1993.

[18] R. Kaune, J. Hörst, and W. Koch, "Accuracy analysis for TDOA localization in sensor networks," in *Proc. 14th Int. Conf. Inf. Fusion*, 2011, pp. 1–8.

[19] W. C. Kim, T. L. Song, and D. Mušicki, "Mobile emitter geolocation and tracking using correlated time difference of arrival measurements," in *Proc. 15th Int. Conf. Inf. Fusion*, 2012, pp. 700–706.

[20] Y. Bar-Shalom, X. R. Li, and T. Kirubarajan, *Estimation with Applications to Tracking and Navigation: Theory Algorithms and Software*. Hoboken, NJ, USA: Wiley, 2004.

[21] Z. Duan, C. Han, and T. Tao, "Optimal multi-sensor fusion target tracking with correlated measurement noises," in *Proc. IEEE Int. Conf. Syst., Man Cybern.*, Oct. 2004, pp. 1272–1278.

[22] M. D. Gillette and H. F. Silverman, "A linear closed-form algorithm for source localization from time-differences of arrival," *IEEE Signal Process. Lett.*, vol. 15, pp. 1–4, Jan. 2008.

[23] A. Beck, P. Stoica, and J. Li, "Exact and approximate solutions of source localization problems," *IEEE Trans. Signal Process.*, vol. 56, no. 5, pp. 1770–1778, May 2008.

[24] S. Challa, D. Musicki, M. R. Morelande, and R. J. Evans, *Fundamentals of Object Tracking*. Cambridge, U.K.: Cambridge Univ. Press, 2011.

[25] R. Karlsson, T. Schön, and F. Gustafsson, "Complexity analysis of the marginalized particle filter," *IEEE Trans. Singnal Process.*, vol. 53, no. 11, pp. 4408–4411, Nov. 2005.

[26] B. Ristic, S. Arulampalam, and N. J. Gordon, *Beyond the Kalman Filter: Particle Filters for Tracking Applications*. Norwood, MA, USA: Artech House, 2004.

HYUNG JUNE KIM was born in Daejeon, South Korea, in 1988. He received the B.Sc. degree in electronic engineering from Hanyang University, Ansan, South Korea, in 2014, where he is currently pursuing the Ph.D. degree. His research interests include target state estimation, multitarget tracking, and multi-sensor data fusion.

YIFAN XIE was born in Hubei, China, in 1992. He received the B.E. degree in electronic information engineering from the Wuhan University of Science and Technology, China, in 2014. He is currently pursuing the Ph.D. degree with Hanyang University, South Korea. His research interests include target tracking and information fusion.

CHANKIL LEE received the B.A. degree from Hanyang University, South Korea, in 1981, the M.S. degree in electronics from Seoul National University, South Korea, in 1983, and the Ph.D. degree in electrical engineering from the Georgia Institute of Technology, USA, in 1992. He is currently serving as a Full Professor and the Head of the Electronics and Communications Engineering Department, Hanyang University. He was a Senior Researcher with ETRI, where he accomplished the design and development of TDX-1 ESS and CDMA cellular communication systems. Based on these research experiences, he has published various papers related to wireless sensor networks and target tracking.

HEEKWON YANG received the B.S. degree in electrical engineering from Koreatech University, in 2002, and the M.S. degree in electronics and communication engineering from Hanyang University, in 2012, where he is currently pursuing the Ph.D. degree. His research activities and interests include a wide range of subjects related to the Internet of Things, wireless sensor networks, big data, cloud computing, edge computing, and a high-precision UWB localization systems.

TAEK LYUL SONG was born in Andong, South Korea, in 1952. He received the B.Sc. degree in nuclear engineering from Seoul National University, Seoul, South Korea, in 1974, and the M.Sc. and Ph.D. degrees in aerospace engineering from The University of Texas at Austin, in 1981 and 1983, respectively. From 1974 to 1994, he was with the Agency for Defense Development, where his major research topics included missile guidance and control and control systems design, target tracking, and navigation systems analysis. He has been a Professor with the Electronic Systems Engineering Department, Hanyang University, since 1995. His research interests include target state estimation, guidance, navigation, and control.

• • •